Electronic Supplementary Material (ESI) for Chemical Science.
This journal is © The Royal Society of Chemistry 2014

Supporting Information

Diaryldichalcogenide Radical Cations

Ole Mallow,[a] Monther A. Khanfar,[b,c] Moritz Malischewski,[b] Pamela Finke,[a] Malte Hesse,[a] Enno Lork,[a] Timo Augenstein,[d] Frank Breher,[d] Jeffrey R. Harmer,[e] Nadezhda V. Vasilieva,[f] Andrey Zibarev,[f,g] Artem S. Bogomyakov,[h] Konrad Seppelt[b] and Jens Beckmann[a]

[*] Correspondence to Jens Beckmann (E-mail: j.beckmann@uni-bremen.de)

Experimental

All reactions and manipulations were carried out under an atmosphere of dry argon using standard Schlenk techniques and glove boxes. All solvents were dried over the appropriate desiccants and freshly distilled prior to use.

Materials and Reagents

The starting materials $(C_6F_5S)_2$ (**13a**),[S1] $(C_6F_5Se)_2$ (**13b**),[S2] $(C_6F_5Te)_2$ (**13c**),[S3] $(2,6\text{-}Mes_2C_6H_3Te)_2$ (**16a**)[21] were prepared according to literature procedures, whereas AsF_5 was obtained by fluorination of elemental As. The SbF_5 was purchased from commercial suppliers and distilled once prior to use. The $[NO][SbF_6]$ was obtained from Sigma-Aldrich and used as received.

Instrumentation and Measurement

CYCLIC VOLTAMETRY. The CV measurements on 0.5 mM solutions of **16a-16c** in CH_2Cl_2 were performed with a PG 310 USB potentiostat (HEKA Elektronik) at 298 K in an argon atmosphere at a stationary Pt electrode (S = 0.08 cm^2) with 0.1 M *n*-Bu_4NBF_4 as a supporting electrolyte. The sweep rates were $0.1 < \nu < 1.2$ $V \cdot s^{-1}$. Peak potentials are quoted with reference to a saturated calomel electrode (SCE). For **16a-16c**, oxidation peaks were diffusion-controlled, i.e. $I_p^{ox}\ \nu^{-0.5} = \text{const.}$, where I_p^{ox} is the peak current (see also Figure S1 and Table S1).

UV-VIS SPECTROSCOPY. UV-vis measurements were carried out using a THERMO-Scientific Genesys 10S at a range between 200 and 800 nm (see also Figures S2-S7).

ELECTROSPRAY MASS SPECTROMETRY. The ESI MS spectra were obtained with a Bruker Esquire-LC ion trap MS. Acetonitrile solutions ($c = 1 \cdot 10^{-6}$ mol L^{-1}) were injected directly into the spectrometer at a flow rate of 3 μL min^{-1}. Nitrogen was used both as a drying gas and for nebulization with flow rates of approximately 5 L min^{-1} and a pressure of 5 psi, respectively. Pressure in the mass analyser region was usually about $1 \cdot 10^{-5}$ mbar. Spectra were collected for one minute and averaged. The nozzle-skimmer voltage was adjusted individually for each measurement (see Figure S8).

ELECTROLYTIC CONDUCTIVITY. All conductivity measurements have been carried out with a WTW Cond 330i at 25°C.

NMR SPECTROSCOPY. The ^{1}H, ^{13}C, ^{77}Se and ^{125}Te NMR spectra were recorded at r.t. (unless otherwise stated) using a Bruker Avance-360 spectrometer and are referenced to Me_2Se (^{77}Se) and Me_2Te (^{125}Te). As secondary references, solutions of 100 mg samples of Ph_2Se_2 (δ (^{77}Se) 464.0 ppm) in $CDCl_3$ and $Te(OH)_6$ (δ (^{125}Te) 707.0 ppm) in D_2O were used.

EPR SPECTROSCOPY. X-band CW EPR experiments were performed on a Bruker BioSpin GmbH E500 spectrometer equipped with a high sensitivity Bruker probe head, and Q-band pulse EPR experiments were carried out on a Bruker X-/Q E580 spectrometer. Both instruments were equipped with Oxford Instruments helium-flow cryostats. The field was calibrated with DPPH (2,2-diphenyl-1-picrylhydrazyl, $g = 2.0036$). The X-band CW EPR spectra were recorded as follows: **17a**: 35 K, 9.400457 GHz, modulation frequency 100 kHz, modulation amplitude 0.05 mT, microwave power 0.003157 mW (48 dB); **17b**: 35 K, 9.401650 GHz, modulation frequency 100 kHz, modulation amplitude 0.2 mT, microwave power 1.992 mW (20 dB); **17c**: 35 K, 9.402240 GHz, modulation frequency 100 kHz, modulation amplitude 0.3 mT, microwave power 9.985 mW (13 dB). Q-band FID-detected field-sweep EPR spectra for **17a** (**17b**) were recorded at 34.1923 GHz, 40 K (34.2476 GHz, 20 K) by integrating over the FID created from a single pulse of length 1000 ns (800 ns). The Q-band (34.1546 GHz) echo-detected field-sweep EPR spectrum of **17c** was recorded at 10 K by integrating the echo (fwhh) from the two-pulse echo sequence π/2 - τ - π - τ - echo, with $t_{\pi/2} = 24$ ns, $t_\pi = 48$ ns, and $\tau = 200$ ns. Q-band Davies ENDOR spectra were recorded at 40 K for **17a**, 12.5 K or **17b** and 10 K for **17c**. All ENDOR data were acquired using the microwave pulse sequence π - T - π/2 - τ - π - τ - echo with mw pulses of lengths $t_{\pi/2} = 40$ ns and $t_\pi = 80$ ns, with $\tau = 240$ ns. During time $T = 20$ μs a radio frequency (rf) pulse of 19 μs was applied stochastically using 80% gain of a 150 W Applied Engineering rf amplifier. The field-sweep EPR and ENDOR data were simulated with the program EasySpin using the functions pepper and salt, respectively (see also Figures S9-12 and Tables S2 and S3).[S4]

MAGNETIC MEASUREMENTS. The magnetic measurements (Figure S12) on **17a-c** were performed with an MPMS*XL* SQUID magnetometer (Quantum Design) in the temperature range 2-300 K with magnetic field of up to 5 kOe. Samples of complexes was placed in small quartz tubes with teflon caps in glovebox and then quickly moved to an airlock and purged with helium. None of complexes exhibited any field dependence of molar magnetization at low temperatures. Diamagnetic corrections were made using the Pascal constants. The effective magnetic moment was calculated as $\mu_{eff}(T) = [(3k/N_A\mu_B^2)\chi T]^{1/2} \approx (8\chi T)^{1/2}$ (see also Figure S13).

MICROANALYSIS. The CHN analyses were obtained using a EuroVector EA3000.

X-RAY CRYSTALLOGRAPHY. Intensity data were collected on a Bruker Smart 200 diffractometer (**14a**, **14b**, **17a**) and a Siemens P4 diffractometer (**16a**, **17b**, **17c**) using graphite-monochromated Mo-Kα (0.7107 Å) radiation. All structures were solved by direct methods and refined based on F^2 by use of the SHELX program package.[S5] All non-hydrogen atoms were refined using anisotropic displacement parameters. Hydrogen atoms attached to carbon atoms were included in geometrically calculated positions using a riding model. Crystal and refinement data are collected in Table S4. Figures were created using DIAMOND.[S6] The molecular of **16a** is shown in Figures S14. Crystallographic data (excluding structure factors) for the structural analyses have been deposited with the Cambridge Crystallographic Data Centre.

Copies of this information may be obtained free of charge from The Director, CCDC, 12 Union Road, Cambridge CB2 1EZ, UK (Fax: +44-1223-336033; e-mail: deposit@ccdc.cam.ac.uk or http://www.ccdc.cam.ac.uk).

COMPUTATIONAL CHEMISTRY. Several sets of computations were performed. Calculation of the EPR parameters were performed using the ORCA program package at the BP86/def2-TZVP level including the ZORA approximation.[S7] The calculations were performed on previously optimized structures using the TURBOMOLE program package.[S8] The geometries were optimized at the (RI)-B3LYP level in the def2-TZVP basis.[S9] The coordinates of the solid state structures were chosen as starting geometry. Since for these calculations the whole, i.e. non-simplified molecules have been taken into account, the optimized structures were not checked for minima by 2nd derivative (frequency) calculations due to the large number of atoms. The conformational analysis was carried out with the Gaussian09 program.[S10] The methylated *m*-terphenyl-substituents have been simplified to phenyl groups in order to reduce the number of electrons, but also to reduce the number of rotational isomers of the methyl groups which would complicate the finding of the ground state configuration. The pentafluorophenyl compounds have been calculated as such. At first some well-established methods have been tested. It turned out that the MP2 *ab initio* method was too time consuming, frequency calculations took months or did not converge. The DFT Becke3LYP method worked reliably. Alternatively user defined models as proposed for radicals has been tested by using a mixed ratio of exact and DFT energy terms of 4.428:0.572 with the MPW1PW91 hybrid functional.[S11] The energy separation and overall geometry of the dichalcogenide radical cations in C_2 and C_s symmetry did not change, so that all further calculations have been performed with the Becke3LYP functional. On the neutral diaryl dichalcogenides the choice of the basis sets has been tested, since their molecular structures are known from X-ray crystallography. The cc-pvTZ basis set is superior to 6-311+G(d,p) in reproducing bond distances. Remaining large differences between experimental and calculated structure are found only for the C-S-S-C and C-Se-Se-C dihedral angles of the fluorinated phenyl derivatives. Basis sets used for selenium are all electron 6-311+G(d,p) and cc-pvTZ, and also a core potential for 28 electron and a 14s10p2d1f[3s3d2p1f] basis set. Te has been represented by a 46 electron core potential and a 15s11p3d1f[3s3p2d1f] basis set.[S12] Wiberg bond indices (WBIs) were calculated with NBO 5.9 as implemented in Gaussian09.[37] The ^{77}Se and ^{125}Te NMR chemical shifts were computed with the GIAO method using the cc-pVTZ basis set for C and H atoms as well as an IGLO-II type basis set for Se and Te (see also Figure S15 and S16 as well as Tables S5-9).[S13]

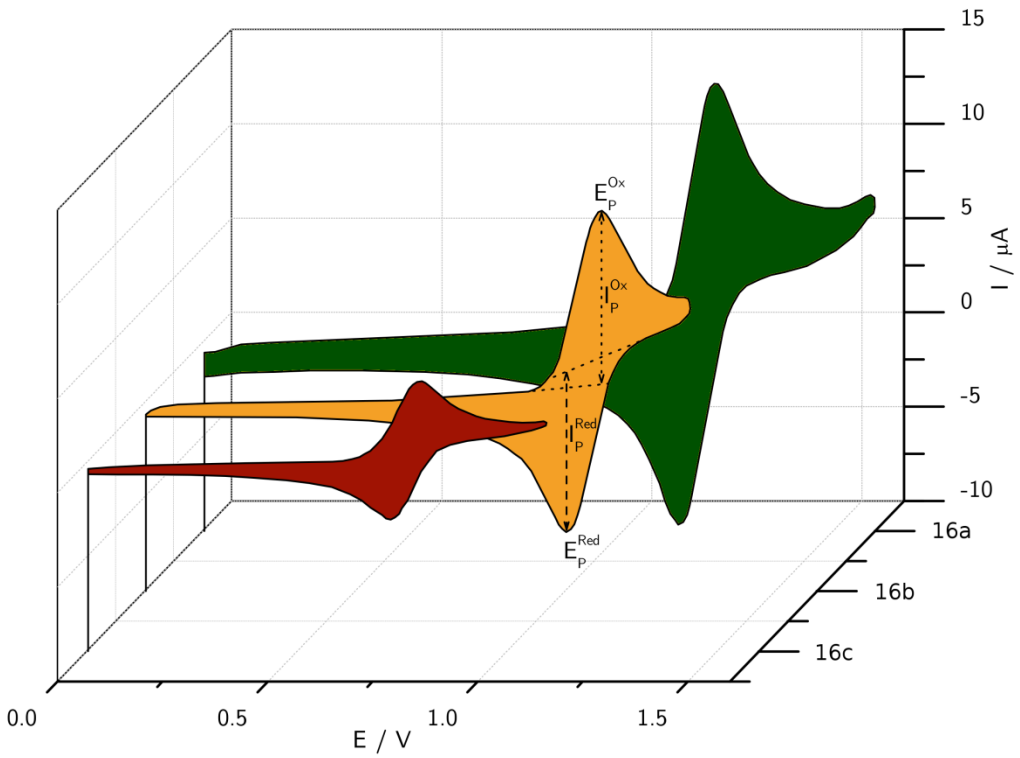

Figure S1. Cyclic voltammograms of **16a-c** at Pt anode in CH_2Cl_2 / 0.1 M n-Bu_4NBF_4 at ν = 0.1 V s^{-1} and c = $5 \cdot 10^{-4}$ mol l^{-1}.

Table S1. Results of the cyclic voltammetry investigations of **16a-c** (ν = 0.1 V s^{-1}, c = $5 \cdot 10^{-4}$ mol l^{-1}).

Compound	E_p^{Ox} / V	E_p^{Red} / V	I_p^{0x} / µA	I_p^{Red} / µA
16a	1.22	1.15	13.2	–11.8
16b	1.09	1.01	9.8	–8.4
16c	0.79	0.71	4.4	–3.6

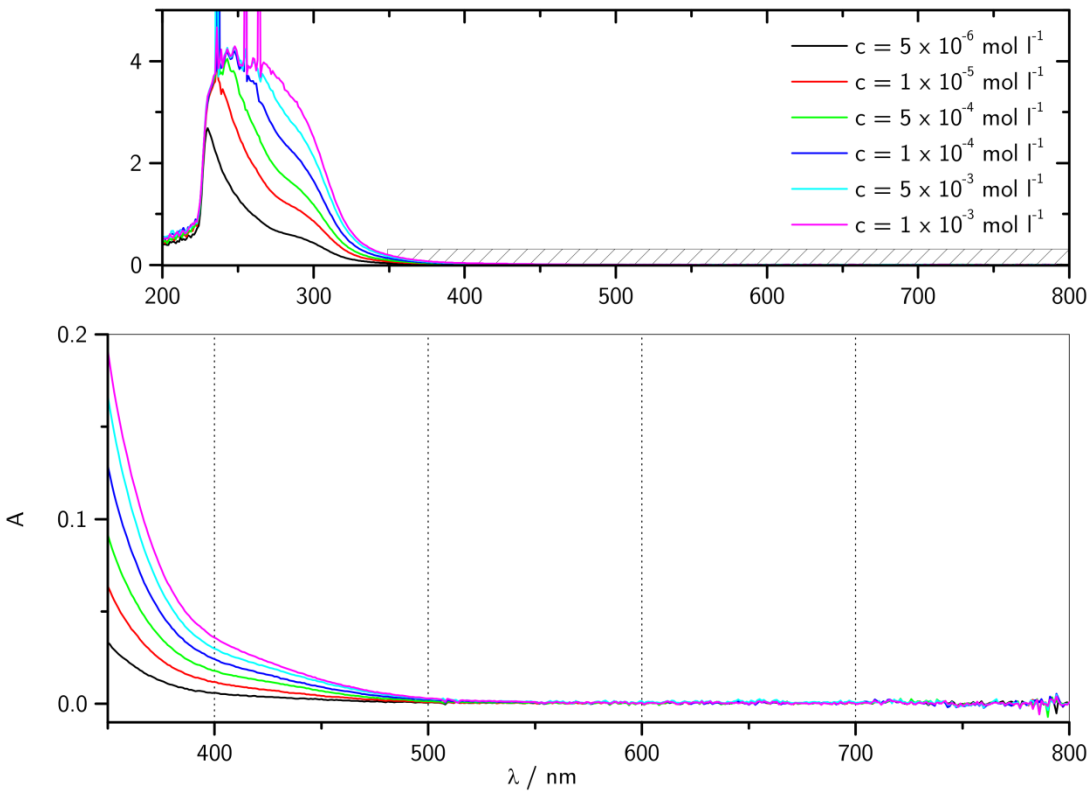

Figure S2. UV/vis spectra of **16a** at various concentrations in CH_2Cl_2.

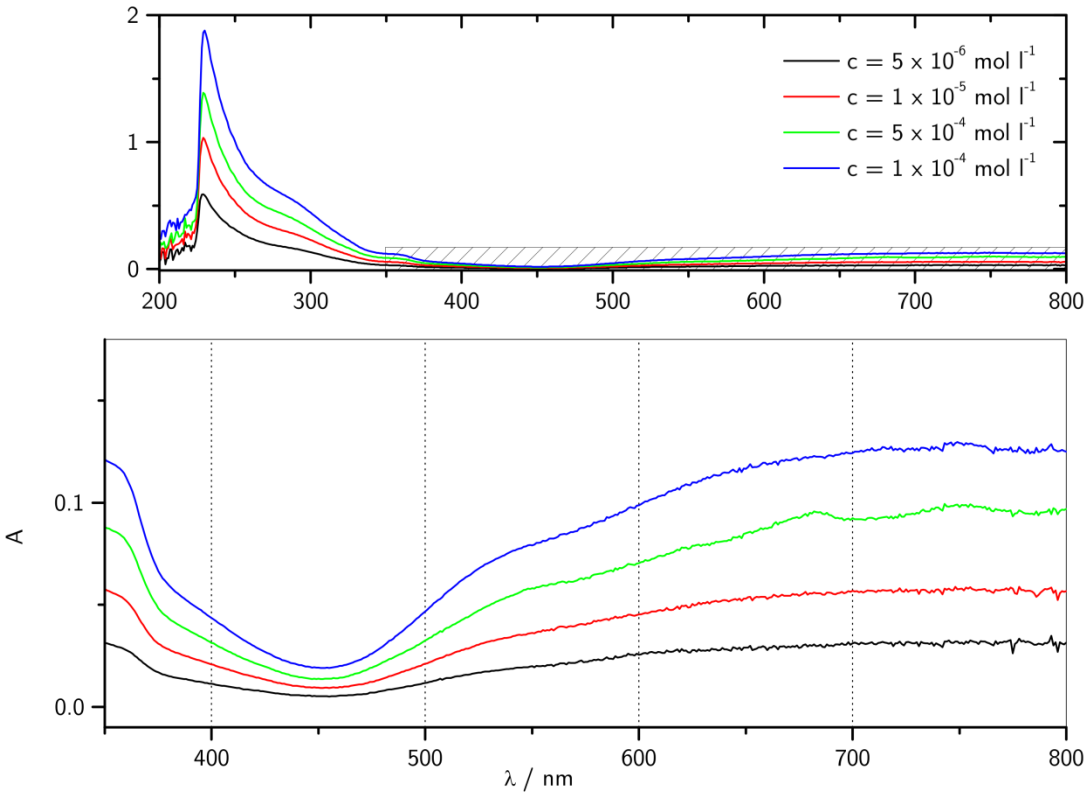

Figure S3. UV/vis spectra of **17a** at various concentrations in CH_2Cl_2.

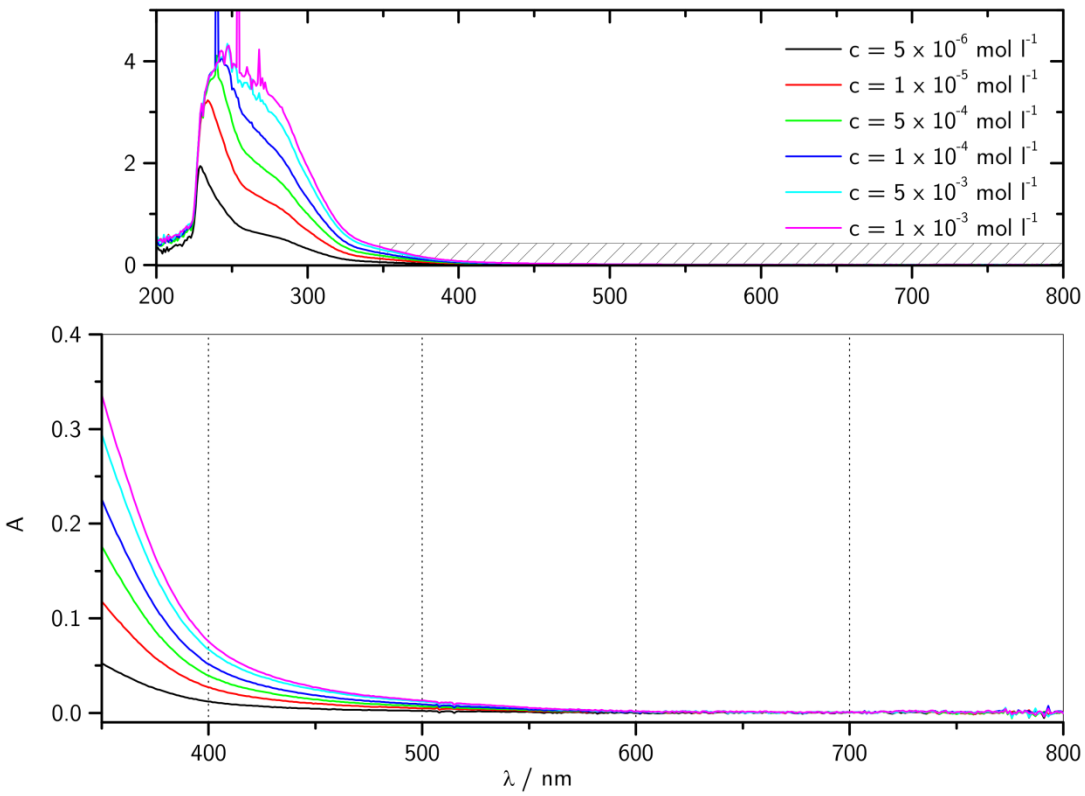

Figure S4. UV/vis spectra of **16b** at various concentrations in CH_2Cl_2.

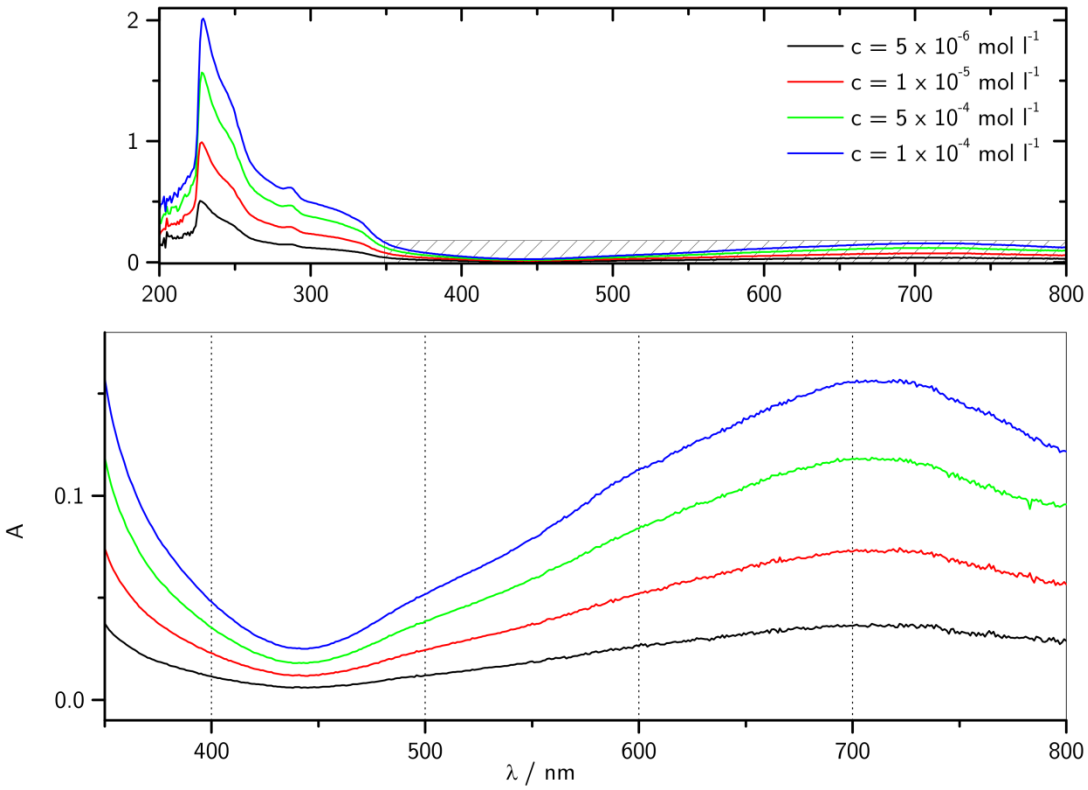

Figure S5. UV/vis spectra of **17b** at various concentrations in CH_2Cl_2.

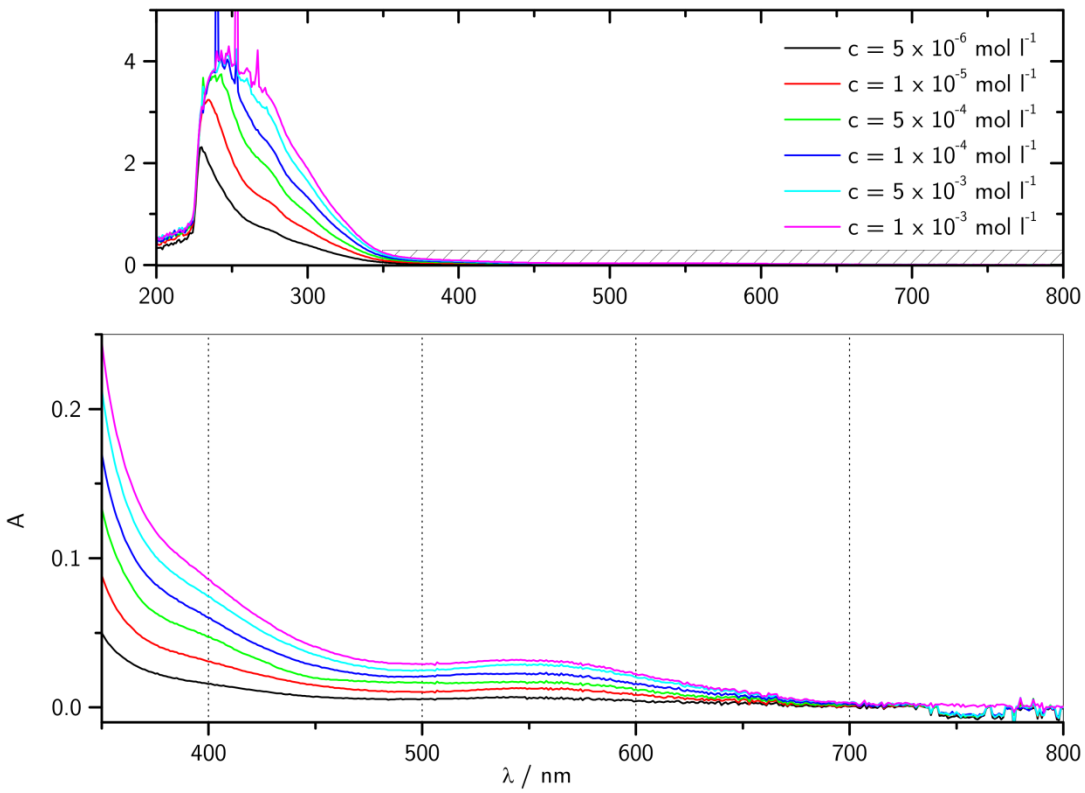

Figure S6. UV/vis spectra of **16c** at various concentrations in CH_2Cl_2.

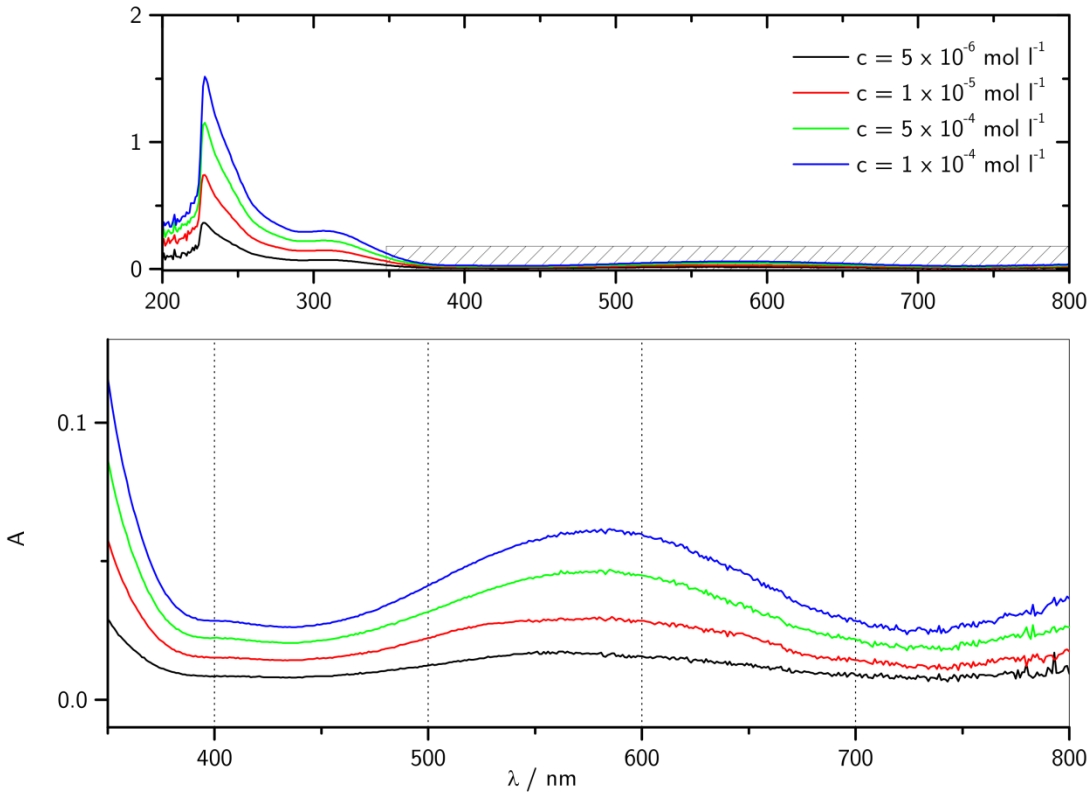

Figure S7. UV/vis spectra of **17c** at various concentrations CH_2Cl_2.

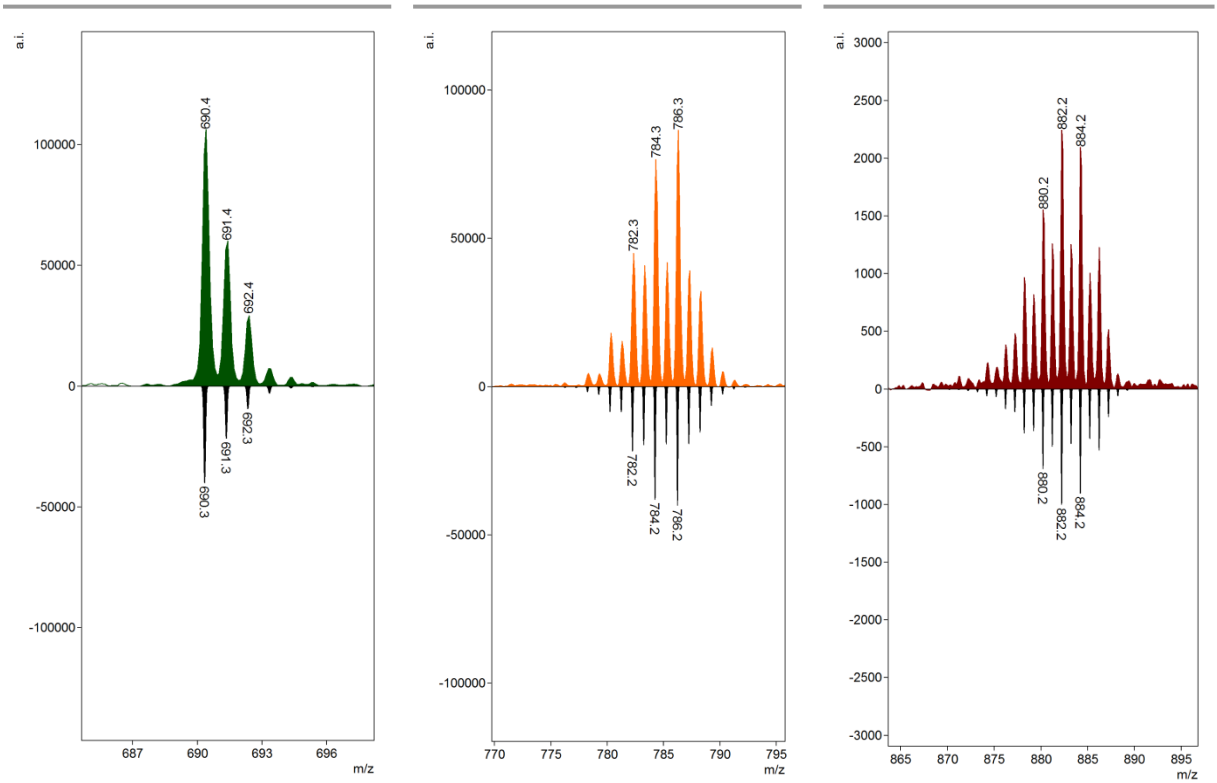

Figure S8. ESI MS spectra (positive mode, MeCN) of **17a-c** showing the experimental (above) and simulated (below) mass clusters of the radical cations.

Table S2: Experimental and DFT (in parentheses) EPR parameters for **17a-c**.

Parameter	Principal values / MHz	Euler angles / deg.	ρ_s	ρ_p	ρ_{total}
		17a			
g	2.0014, 2.0115, 2.0285		-	-	-
	(2.0022, 2.0107, 2.0213)	(0,0,0)			
A(^{1}H)	-3.0, -7.2, -11.0			n.a.	
	(-1.8, -5.8, -8.5)	(3.1, 93.1,92.8)	*(-0.00131)*		*(-0.00131)*
L	7.5, 7.5, 10 (X-band) / 9, 9, 22 (Q-band)		-	-	-
		17b			
g	1.9956, 2.0438, 2.1543		-	-	-
	(2.0021, 2.0452, 2.1165)	(0,0,0)			
A(^{77}Se)	-50, -100, 465				
	(-106, -116, 306)	(-2.0,88.5,0.2)	*(0.00259)*	*(0.33175)*	*(0.33228)*
A(^{77}Se)	-80, -115, 610				
	(-135, -140, 407)	(4.0,91.0,-0.2)	*(0.00332)*	*(0.39967)*	*(0.40193)*
A(^{1}H)	-1.8, -4.3, -6.4			n.a.	
	(-1.2, -4.2, -6.1)	(-1.3,85.0,85.3)	*(-0.00080)*		*(-0.00080)*
L	15, 18, 40 (X-band) / 15, 30, 120 (Q-band)		-	-	-
		17c			
g	1.9542, 2.0411, 2.4566		-	-	-
	(2.0021, 2.0876, 2.3688)	(0,0,0)			
A(^{127}Te)	300, 350, -1000				
	(350, 370, -720)	(-179.6,82.2,-179.0) (-	*(0.00085)*	*(0.39122)*	*(0.38784)*
	(352, 372, -724)	179.6,97.7,179.0)	*(0.00089)*	*(0.39312)*	*(0.38970)*
A(^{1}H)	- , - , -3.8			n.a.	
	(-0.6, -2.6, -3.8)	(-174.9,94.8,-110.3)	*(-0.00042)*		*(-0.00042)*
L	30, 30, 90 (X-band) / 120, 120, 220 (Q-band)		-	-	-

Listed are the principal *g*-values *g*, principal hyperfine values *A* (MHz) and their corresponding Euler angles (degrees), X- and Q-band linewidths *L* (MHz) for the EPR simulations, and the spin densities in s-type ρ_s and p-type ρ_p orbitals and their sum. All simulations used Euler angles from the DFT calculations, and the sign of the experimental hyperfine couplings are assigned to be consistent with the DFT results (experiment data provide only absolute values).

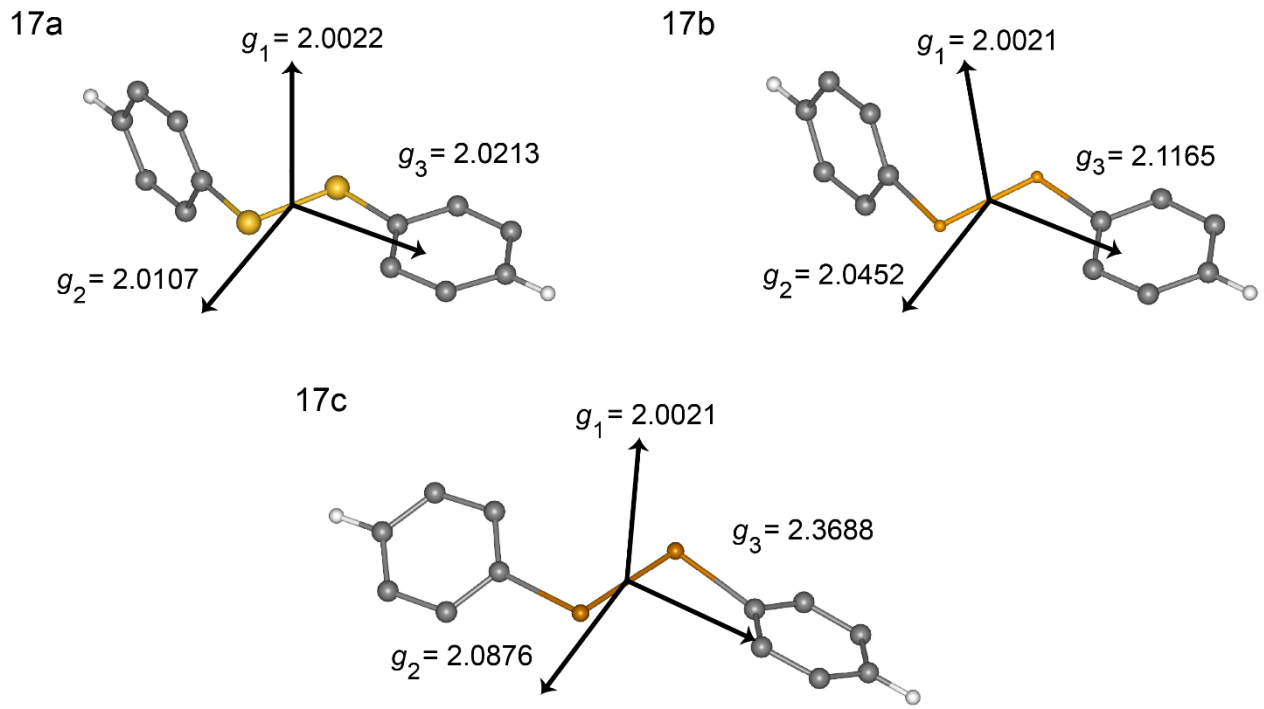

Figure S9. Orientation of the g-matrix axes in the Molecular frame for radicals **17a**, **17b** and **17c** (see also Table S3).

Table S3. g-matrix principal axis vectors g_1, g_2, g_3 for the radicals **17a**, **17b** and **17c** in the molecular frame (defined by the selected atom coordinates below) from the DFT calculations (see also Figure S9).

	17a				**17b**				**17c**		
g_1	-0.186	-0.9471	-0.2616	g_1	-0.081	-0.8945	-0.4396	g_1	0.737	0.6759	0.0049
g_2	0.9753	-0.2103	0.0681	g_2	0.9745	-0.1637	0.1536	g_2	0.6608	-0.722	0.205
g_3	-0.1195	-0.2424	0.9628	g_3	-0.2094	-0.416	0.885	g_3	0.1421	-0.1479	-0.9787
C	0.2095	2.3735	-3.6619	C	3.0536	1.6446	-3.4331	C	0.7929	-0.3842	-3.2613
C	0.5682	1.9271	-2.3727	C	2.6871	1.0312	-2.2222	C	0.7976	-0.6965	-4.6407
C	-0.2313	1.4675	-4.6391	C	2.071	2.0847	-4.3338	Te	-0.6381	1.0407	-0.7277
C	0.448	0.5399	-2.1028	C	1.3021	0.8698	-1.9341	C	-0.3361	0.3089	-2.7521
S	1.0087	-0.0664	-0.4977	Se	1.0865	-0.0122	-0.2234	Te	0.9712	-0.729	0.6702
C	-0.3123	0.0951	-4.3543	C	0.7119	1.9123	-4.03	C	-0.2648	-0.3357	-5.4815
C	0.0362	-0.4019	-3.0813	C	-1.3451	-0.5724	4.3938	C	-0.3115	0.8156	3.2128
C	0.5197	-0.8801	2.838	C	-1.1353	-1.9505	4.557	C	-1.4203	0.6883	-3.5901
S	-0.8745	0.0188	0.4768	C	-1.3387	0.0071	3.1079	C	-1.3682	0.3535	-4.9582
C	0.4362	-1.1476	4.2202	C	0.2881	1.301	-2.8292	C	0.2636	-0.3737	2.6947
C	-0.665	-0.4247	2.1928	C	-0.9301	-2.7751	3.4403	C	-0.6125	0.8455	4.5943
C	-0.7612	-0.988	4.9354	C	-1.1067	-0.8439	1.9986	C	0.5338	-1.4959	3.5248
C	-1.8971	-0.2632	2.9001	C	-0.9201	-2.245	2.1318	C	-0.353	-0.251	5.4286
C	-1.9207	-0.5512	4.2745	Se	-1.2503	-0.0166	0.2375	C	0.2164	-1.4161	4.8956

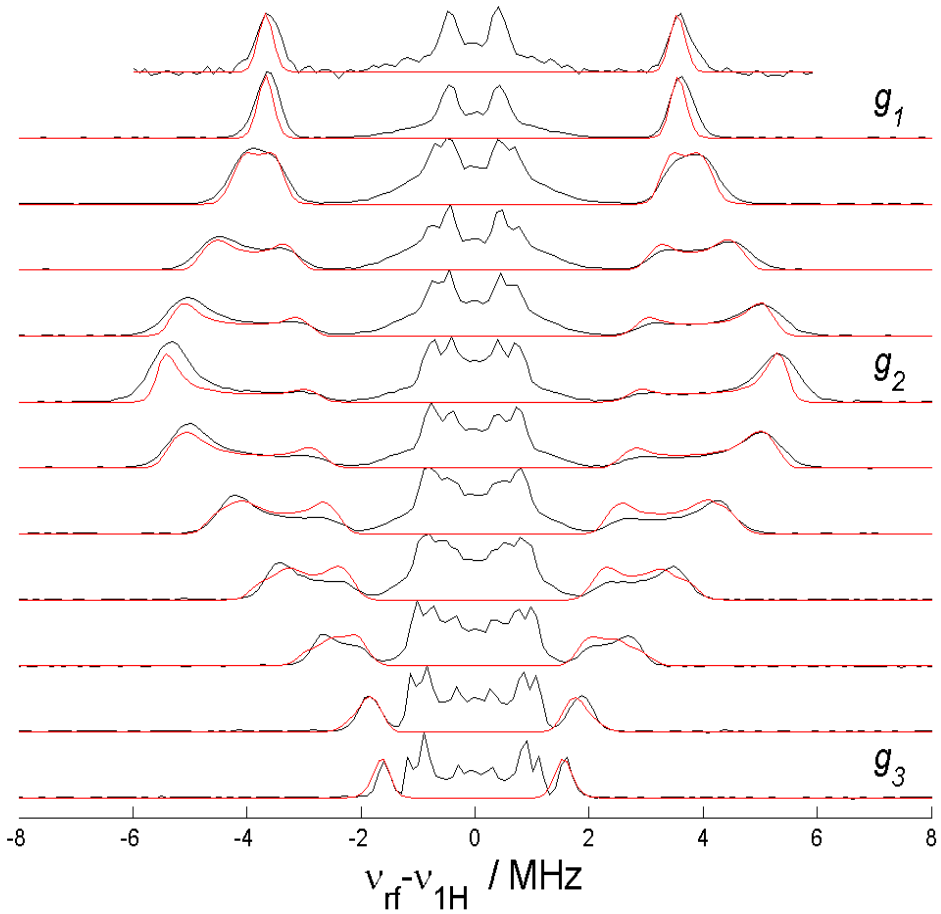

Figure S10. ^{1}H Q-band (34.1922 GHz) Davies ENDOR spectra recorded at 40 K of **17a** (black) and simulations (red) for the largest proton hyperfine coupling (the one resolved in the EPR spectra). Spectra have been centred around the ^{1}H Larmor frequency ν_{1H}. The measurement field positions from bottom (g_3) to top (g_1) are: 1204.7 (~g_3), 1205.7, 1207.7, 1209.7, 1211.7, 1213.7, 1214.5 (~g_2), 1215.6, 1217.2, 1218.9, 1220.6 (~g_1), 1221.0 mT.

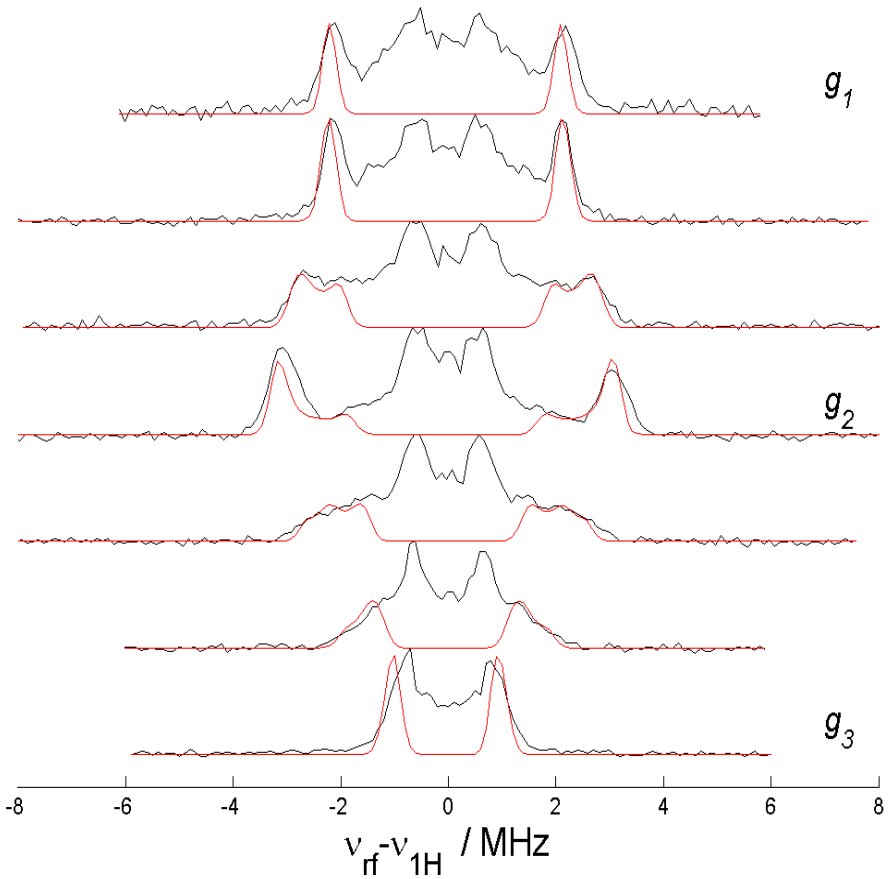

Figure S11. ^{1}H Q-band (34.2443 GHz) Davies ENDOR spectra recorded at 12.5 K for **17b** (black) and simulations (red) for the largest proton hyperfine coupling. Spectra have been centred around the ^{1}H Larmor frequency ν_{1H}. The measurement field positions from bottom (g_3) to top (g_1) are: 1139.2 (~g_3), 1158.3, 1177.4, 1197.2 (~g_2), 1207.2, 1223.7, 1228.7 mT (~g_1).

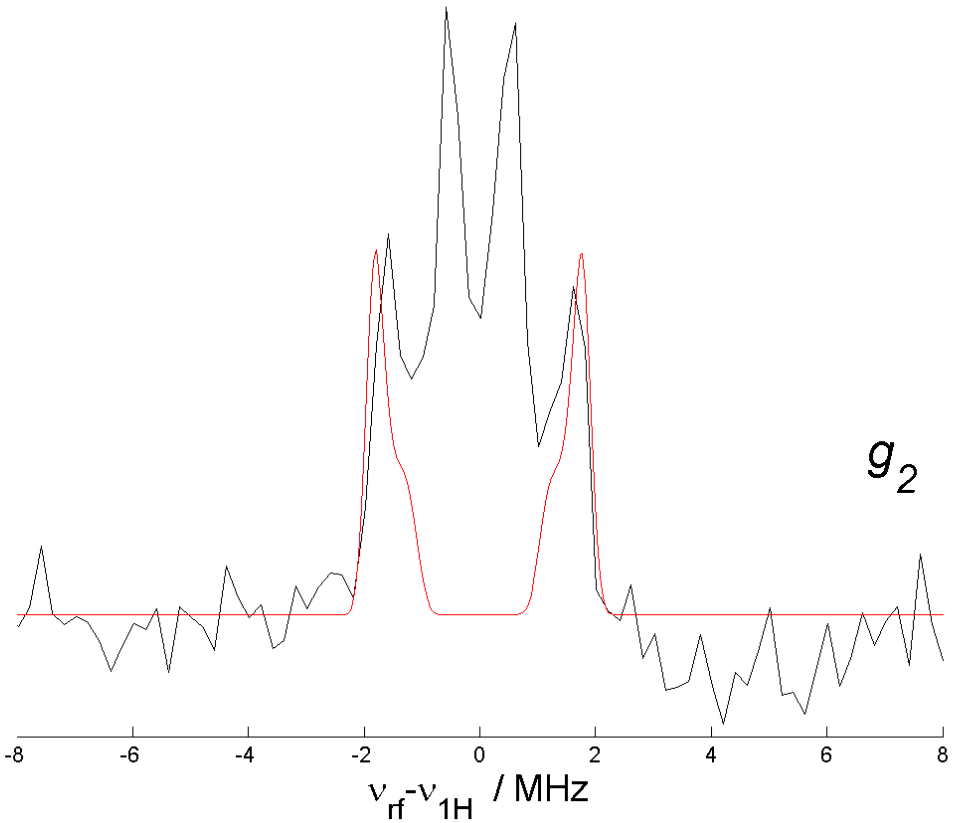

Figure S12. ^{1}H Q-band (34.1545 GHz) Davies ENDOR spectrum recorded at 10 K of **17c** (black) and simulation (red) for the largest proton coupling. The observer position was close to g_2 (B_0 = 1195.1 mT) and shows the largest coupling is $|A_{max}|$ = 3.8 MHz.

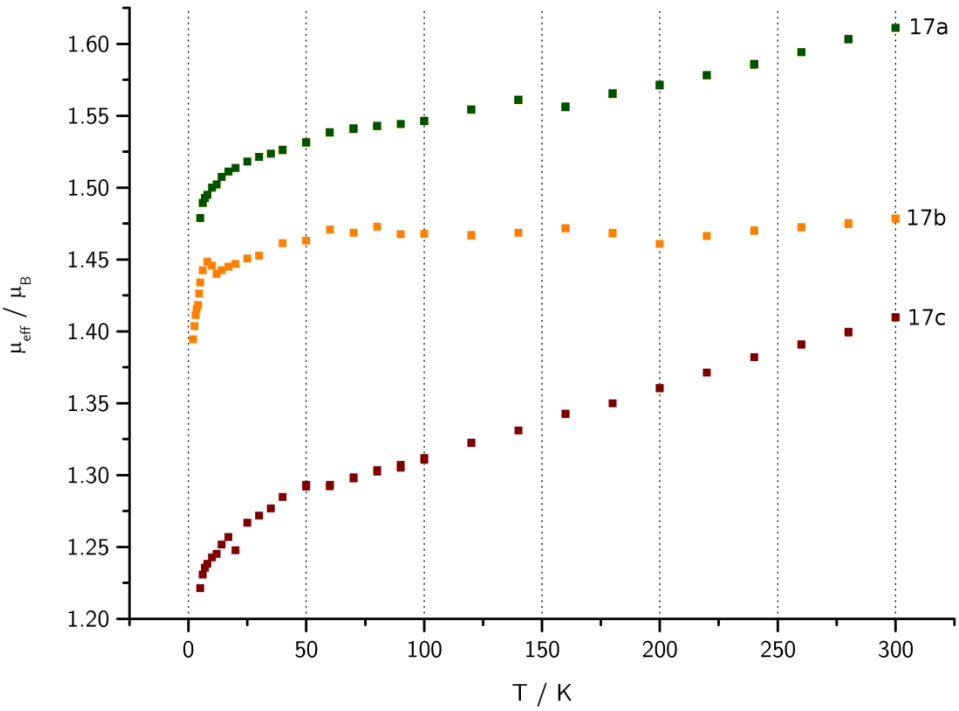

Figure S13. Temperature dependences of effective magnetic moment μ_{eff} of **17a-c**.

Table S4. Crystal data and structure refinement of [**14b**][As_2F_{11}], **16a**, [**17a-c**][SbF_6],

	[**14a**][Sb_2F_{11}]	[**14b**][As_2F_{11}]	**16a**
Formula	$C_{12}F_{21}S_2Sb_2$	$C_{12}As_2F_{21}Se_2$	$C_{48}H_{50}S_2$
Formula weight, g mol^{-1}	850.74	850.88	691.00
Crystal system	monoclinic	triclinic	monoclinic
Crystal size, mm	0.2×0.05×0.02	0.6×0.4×0.02	0.9×0.8×0.6
Space group	$P2_1/n$	P-1	$P2_1/n$
a, Å	12.029(4)	8.5406(18)	15.695(3)
b, Å	12.276(6)	8.5891(18)	15.264(2)
c, Å	14.440(7)	14.093(3)	16.274(2)
α, º	90.00	84.900(5)	90
β, º	97.662(14)	84.781(5)	93.450(10)
γ, º	90.00	88.091(5)	90
V, Å^3	2113.3(16)	1025.1(4)	3892(1)
Z	4	2	4
ρ_{calcd}, Mg m^{-3}	2.674	2.757	1.179
μ (Mo $K\alpha$), mm^{-1}	2.938	7.000	0.169
F(000)	1580	790	1480
θ range, deg	2.07 to 26.13	2.38 to 30.60	2.51 to 27.50
Index ranges	$-14 \le h \le 14$	$-11 \le h \le 12$	$-19 \le h \le 20$
	$-15 \le k \le 16$	$-12 \le k \le 12$	$-19 \le k \le 13$
	$-1 \le l \le 17$	$-20 \le l \le 17$	$-21 \le l \le 21$
No. of reflns collected	4165	16040	10766
Completeness to θ_{max}	99.0%	96.8%	99.7%
No. indep. Reflns	4165	6115	8906
No. obsd reflns with ($I>2\sigma(I)$)	2858	4844	5949
No. refined params	335	334	463
GooF (F^2)	1.037	1.020	1.013
R_1 (F) ($I > 2\sigma(I)$)	0.0469	0.0264	0.0609
wR_2 (F^2) (all data)	0.1395	0.0660	0.1663
Largest diff peak/hole, e Å^{-3}	1.229 / –1.138	1.379 / –0.579	0.378 / –0.433
CCDC number	1028017	999869	999870

Table S4. Cont.

[**17a**][SbF_6]	[**17b**][SbF_6]·CH_2Cl_2	[**17c**][SbF_6]·$NCCH_2CH_3$
$C_{48}H_{50}F_6S_2Sb$	$C_{49}H_{52}Cl_2F_6SbSe_2$	$C_{51}H_{55}F_6NSbTe_2$
926.75	1105.48	1172.91
monoclinic	monoclinic	monoclinic
0.1×0.05×0.05	0.7×0.6×0.3	1.0×0.2×0.2
$P2_1/n$	$P2_1/c$	$P2_1/c$
16.170(3)	19.147(6)	19.854(5)
15.837(3)	15.238(5)	14.726(3)
17.339(4)	16.653(9)	17.178(9)
90	90	90
92.97(3)	90.08(3)	92.07(4)
90	90	90
4434(2)	4859(3)	5019(3)
4	4	4
1.388	1.511	1.552
0.774	2.231	1.745
1900	2212	2308
2.61 to 27.50	2.13 to 25.02	2.50 to 22.51
$-17 \le h \le 17$	$-22 \le h \le 22$	$-21 \le h \le 13$
$-17 \le k \le 17$	$-18 \le k \le 14$	$-13 \le k \le 15$
$-19 \le l \le 29$	$-19 \le l \le 17$	$-18 \le l \le 18$
141590	10289	7572
99.7%	98.7%	99.8%
6341	8445	3281
3793	4836	2304
526	563	281
1.024	1.017	0.985
0.0543	0.0705	0.0523
0.1195	0.1879	0.1346
0.925 / –0.430	1.216 / –1.277	1.516 / –0.988
999871	999872	999873

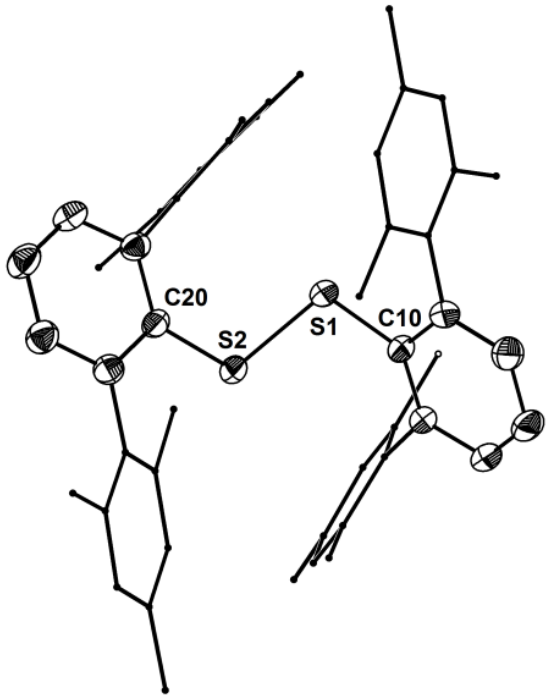

Figure S14. Molecular structure of **16a**; thermal ellipsoids are set at 30% probability.

Table S5. Calculated and experimental structure data of the (neutral) diaryldichalcogens.

	Method	$(PhS)_2$ (**1a**)	$(C_6F_5S)_2$ (**13a**)
E [a.u.]	B3LYP/6-311+G(d,p)	-1259.84941	-2252.43842
	B3LYP/cc-pvTZ	-1259.91375	-2252.57201
E-E [pm]	B3LYP/6-311+G(d,p)	213.0	209.2
	B3LYP/cc-pvTZ	205.5	207.2
	X-ray structure	202.7[S14]	205.9[S15]
E-C [pm]	B3LYP/6-311+G(d,p)	179.5	179.5
	B3LYP/cc-pvTZ	179.5	179.1
	X-ray structure	178.9[S14]	177.0[S15]
E-E-C [°]	B3LYP/6-311+G(d,p)	104.6	106.1
	B3LYP/cc-pvTZ	106.8	106.6
	X-ray structure	106.1[S14]	101.5[S15]
C-E-E-C [°]	B3LYP/6-311+G(d,p)	82.5	103.8
	B3LYP/cc-pvTZ	90.8	106.6
	X-ray structure	84.3[S14]	76.5[S15]

	Method	$(PhSe)_2$ (**1b**)	$(C_6F_5Se)_2$ (**13b**)
E [a.u.]	B3LYP/6-311+G(d,p)	-5266.52869	-6259.13448
	B3LYP/cc-pvTZ	-5266.73608	-6259.40913
E-E [pm]	B3LYP/6-311+G(d,p)	234.3	237.7
	B3LYP/cc-pvTZ	233.2	236.6
	X-ray structure	230.7[S14]	231.9[S15]
E-C [pm]	B3LYP/6-311+G(d,p)	195.2	193.4
	B3LYP/cc-pvTZ	194.7	192.9
	X-ray structure	194.2[S14]	191.0[S15]
E-E-C [°]	B3LYP/6-311+G(d,p)	104.1	101.4
	B3LYP/cc-pvTZ	104.5	101.9
	X-ray structure	103.5[S14]	98.7[S15]
C-E-E-C [°]	B3LYP/6-311+G(d,p)	91.4	87.5
	B3LYP/cc-pvTZ	91.5	89.6
	X-ray structure	85.4[S14]	75.3[S15]

	Method	$(PhTe)_2$ (**1c**)	$(C_6F_5Te)_2$ (**13c**)
E [a.u.]	B3LYP/6-311+G(d,p)	-479.60581	-1472.21825
	B3LYP/cc-pvTZ	-479.64947	-1472.32215
E-E [pm]	B3LYP/6-311+G(d,p)	268.2	270.1
	B3LYP/cc-pvTZ	268.3	270.8
	X-ray structure	270.9[S14]	212.6[S16]
E-C [pm]	B3LYP/6-311+G(d,p)	213.4	212.6
	B3LYP/cc-pvTZ	213.7	213.3
	X-ray structure	212.0[S14]	212.4[S16]
E-E-C [°]	B3LYP/6-311+G(d,p)	102.3	100.1
	B3LYP/cc-pvTZ	102.5	103.2
	X-ray structure	100.6[S14]	98.6[S16]
C-E-E-C [°]	B3LYP/6-311+G(d,p)	92.7	88.7
	B3LYP/cc-pvTZ	92.3	112.0
	X-ray structure	90.7[S14]	91.8[S16]

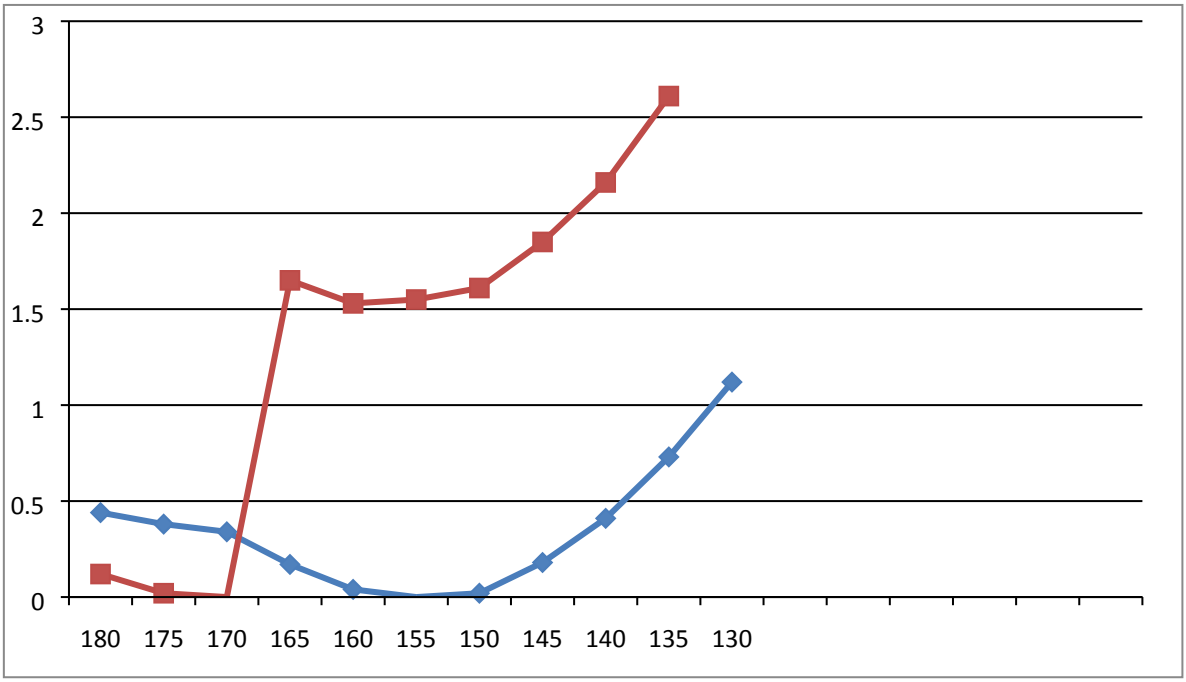

Figure S15. Relaxed potential energy surface scan considering the transitions between the C_2 and the C_s symmetric structures of $(C_6H_5S)_2^{\bullet+}$ (**2a**, blue) and $(C_6F_5S)_2^{\bullet+}$ (**14a**, red) by calculation of relative energies (kcal / mol) at fixed C-S-S-C dihedral angles (varied in 5° steps).

Table S6. Calculated energies (a.u.) of the diphenyl-dichalcogen radical cations and their energetic difference (kcal / mol) between C_s and C_2 (C_{2h} for **14c**) symmetry.

	E_h (a.u.) C_s symmetry	E_h (a.u.) C_2 symmetry	ΔE (kcal/mol)
$[(PhS)_2]^{\bullet+}$ (**2a**)			
B3LYP/6-311+G(d,p)	-1259.57331	-1259.57403	0.45
B3LYP/cc-pvTZ	-1259.64224	-1259.64313	0.55
MPW1K/6-311+G(d,p)	-1259.52391	-1259.52595	1.28
MPW1K/cc-pvTZ	-1259.58801	-1259.59017	1.36
$[(C_6F_5S)_2]^{\bullet+}$ (**14a**)			
B3LYP/6-311+G(d,p)	-2251.13065	-2252.12837	-1.43
B3LYP/cc-pvTZ	-2252.27391	-2251.27178	-1.33
MPW1K/6-311+G(d,p)	-2252.05605	-2252.05451	-0.97
MPW1K/cc-pvTZ	-2251.19019	-2252.18898	-0.95
$[(PhSe)_2]^{\bullet+}$ (**2b**)			
B3LYP/6-311+G(d,p)	-5266.26096	-5266.26147	0.32
B3LYP/cc-pvTZ	-5266.46995	-5266.47045	0.31
B3LYP/6-311+G(d,p)/ecp[a]	-481.88304	-481.88352	0.31
$[(C_6F_5Se)_2]^{\bullet+}$ (**14b**)			
B3LYP/6-311+G(d,p)	-6258.82533	-6258.82262	-1.71
B3LYP/cc-pvTZ	-6259.10831	-6259.10581	-1.56
B3LYP/6-311+G(d,p)/ecp[a]	-1474.44816	-1474.44536	-1.74
$[(PhTe)_2]^{\bullet+}$ (**2c**)			
B3LYP/6-311+G(d,p)/ecp[b]	-479.34761	-479.34854	0.59
B3LYP/cc-pvTZ/ecp[b]	-479.39169	-479.39275	0.61
$[(C_6F_5Te)_2]^{\bullet+}$ (**14c**)			
B3LYP/6-311+G(d,p)/ecp[b]	-1471.92486	-1471.92528	0.26
B3LYP/cc-pvTZ/ecp[b]	-1472.04091	-1472.04151	0.37

(a) Se: rel. corrected core potential for 28 electrons, 14s10p2d1f[3s3p2d1f] basis set.

(b) Te: rel. corrected core potential for 46 electrons, 15s11p3d1f[3s3p2d1f] basis set.

Table S7. Structural data of the diaryldichalcogen radical cations in C_s and C_2 (C_{2h} for **14c**) symmetry, calculated at the B3LYP/cc-pvT level of theory.

	$[(PhS)_2]^{\bullet+}$ (**2a**)		$[(C_6F_5S)_2]^{\bullet+}$ (**14a**)	
Symmetry	C_s	C_2	C_s	C_2
E-E [pm]	205.9	204.9	208.5	206.7
E-C [pm]	178.3, 174.3	176.5	175.8, 173.7	175.4
E-E-C [°]	99.3, 107.0	102.8	97.2, 109.1	101.8
C-E-E-C [°]	180.0	156.9	180.0	159.1

	$(PhSe)_2^{\bullet+}$ (**2b**)		$(C_6F_5Se)_2^{\bullet+}$ (**14b**)	
Symmetry	C_s	C_2	C_s	C_2
E-E [pm]	233.3	232.4	235.4	234.3
E-C [pm]	192.7, 189.8	191.5	190.5, 189.1	190.2
E-E-C [°]	97.0, 105.0	100.0	94.8, 106.4	99.7
C-E-E-C [°]	180.0	161.4	180.0	166.4

	$(PhTe)_2^{\bullet+}$ (**2c**)		$(C_6F_5Te)_2^{\bullet+}$ (**14c**)	
Symmetry	C_s	C_2	C_s	C_{2h}
E-E [pm]	268.7	268.3	270.0	271.5
E-C [pm]	211.1, 209.1	210.4	210.0, 209.0	208.8
E-E-C [°]	94.2, 103.0	97.4	92.5, 102.2	102.2
C-E-E-C [°]	180.0	167.9	180.0	180.0

Table S8. Calculated ionization energies (eV) of the diaryldichalcogens **1a-c** and **13a-c**.

	B3LYP/6-311+G(d,p) Te: core pot. 15s11p3d1f[3s3p2d1f]	B3LYP/cc-pvTZ Te: core pot. 15s11p3d1f[3s3p2d1f]
$(PhS)_2$ (**1a**)	7.49	7.38
$(C_6F_5S)_2$ (**13a**)	8.37	8.11
$(PhSe)_2$ (**1b**)	7.27	7.23
$(C_6F_5Se)_2$ (**13b**)	8.41	8.16
$(PhTe)_2$ (**1c**)	7.01	6.98
$(C_6F_5Te)_2$ (**13c**)	7.79	7.64

Table S9. Wiberg Bond Indices, Natural Charges, and Mullikan Charges at the chalcogen atoms of **1a-c**, **2a-c**, **13a-c** and **14a-c**.

$(RE)_2$ $[(RE)_2]^{\bullet+}$	**1a** and **2a** E = S R = Ph	**13a** and **14a** E = S R = C_6F_5	**1b** and **2b** E = Se R = Ph	**13b** and **14b** E = Se R = C_6F_5	**1c** and **2c** E = Te R = Ph	**13c** and **14c** E = Te R = C_6F_5
WBI (E-E)	1.077	1.057	1.060	1.001	1.085	1.058
	1.216	*1.176*	*1.246*	*1.221*	*1.315*	*1.282*
Natural	0.149	0.198	0.191	0.223	0.308	0.367
charges (E)	*0.320, 0.470*	*0.409, 0.486*	*0.401, 0.552*	*0.509, 0.571*	*0.574, 0.712*	*0.723*
Mullikan	-0.010	0.047	0.027	0.101	0.001	0.072
charge (E)	*0.143, 0.255*	0.243, 0.298	*0.242, 0.368*	*0.362, 0.423*	*0.222, 0.305*	*0.398*

Neutral compounds in C_2 symmetry; Radical cations in C_s symmetry, except $(C_6F_5Te)_2^{\bullet+}$ (**14c**) which has C_{2h} symmetry. Second numbers refer to the chalcogen atoms that are linked to the in-plane phenyl rings in case of C_s symmetry. Method Becke3LYP, cc-pVTZ basis sets.

References

S1 A. McKillop, D. Koyunco, A. Krief, W. Dumont, P. Renier, M. Tarabelsi, *Tetrahedron Lett.*, 1990, **31**, 5007.

S2 T. M. Klapötke, B. Krumm, K. Polborn, *Eur. J. Inorg. Chem.*, 1999, 1359.

S3 (a) R. Kasemann, D. Naumann, *J. Fluorine Chem.*, 1990, **48**, 207; (b) T. M. Klapötke, B. Krumm, P. Mayer, K. Polborn, O. P. Ruscitti J., *Fluorine Chem.*, 2001, **112**, 207; (c) T. M. Klapötke, B. Krumm, P. Mayer, D. Naumann, I. Schwab J., *Fluorine Chem.*, 2004, **125**, 997.

S4 S. Stoll, A. Schweiger, *J. Magn. Reson.*, 2006, **178**, 42.

S5 G.M. Sheldrick, *Acta Cryst.*, 2008, **A64**, 112.

S6 K. Brandenburg, H. Putz DIAMOND V3.1d. Crystal Impact GbR, Bonn, Germany, 2006.

S7 F. Neese, *Wiley Interdiscip. Rev.: Comput. Mol. Sci.*, 2012, **2**, 73. D. Ganyushin, F. Neese, *J. Chem. Phys.*, 2013 **138**, 104113.

S8 TURBOMOLE V6.4, a development of Universität Karlsruhe (TH) and Forschungszentrum Karlsruhe GmbH, 1989–2007, TURBOMOLE GmbH, since 2007. Available from http://www.turbomole.com, 2012.).

S9 (a) A. D. Becke, *J. Chem. Phys*., 1993, **98**, 5648; (b) F. Weigend, R. Ahlrichs, *Phys. Chem. Chem. Phys.* 2005, **7**, 3297; (c) F. Weigend, *Phys. Chem. Chem. Phys.* 2006, **8**, 1057.

S10 Gaussian 09, Revision A.02, M. J. Frisch, G. W. Trucks, H. B. Schlegel, G. E. Scuseria, M. A. Robb, J. R. Cheeseman, G. Scalmani, V. Barone, B. Mennucci,G. A. Petersson, H. Nakatsuji, M. Caricato, X. Li, H. P. Hratchian, A. F. Izmaylov, J. Bloino, G. Zheng, J. L. Sonnenberg, M. Hada, M. Ehara, K. Toyota, R. Fukuda, J. Hasegawa, M. Ishida, T. Nakajima, Y. Honda, O. Kitao, H. Nakai, T. Vreven, J. A. Montgomery, Jr., J. E. Peralta, F. Ogliaro, M. Bearpark, J. J. Heyd, E. Brothers, K. N. Kudin, V. N. Staroverov, R. Kobayashi, J. Normand, K. Raghavachari, A. Rendell, J. C. Burant, S. S. Iyengar, J. Tomasi, M. Cossi, N. Rega, J. M. Millam, M. Klene, J. E. Knox, J. B. Cross, V. Bakken, C. Adamo, J. Jaramillo, R. Gomperts, R. E. Stratmann, O. Yazyev, A. J. Austin, R. Cammi, C. Pomelli, J. W. Ochterski, R. L. Martin, K. Morokuma, V. G. Zakrzewski, G. A. Voth, P. Salvador, J. J. Dannenberg, S. Dapprich, A. D. Daniels, O. Farkas, J. B. Foresman, J. V. Ortiz, J. Cioslowski, D. J. Fox, Gaussian, Inc., Wallingford CT, 2009.

S11 B.J. Lynch, P.L. Fast, M. Harris, D.G. Truhlar, *J. Chem. Phys. A*, 2000, **104**, 4811.

S12 J.M.L. Martin, A. Sundermann, *J. Chem. Phys.*, 2001, **114**, 3408.

S13 U. Fleischer, unpublished results, as communicated by M. Kaupp.

S14 A.-L. Fuller, L.S. Scott-Hayward, Y. Li, M. Bühl, A.M.Z. Slawin, J. D. Woollins, *J. Am. Chem. Soc*., 2010, **132**, 5799.

S15 I.Bagryanskaya,Y.V. Gatilov, E. Lork, R. Mews, A.V. Zibarev, *J. Fluor. Chem*., 2006, **127**, 746.

S16 T.M. Klapötke, B. Krumm, P. Mayer, K. Polborn, O.P. Ruscitti, J. Fluor. Chem., 2001, **112**, 207.